

Supporting Information

A Novel Hexanuclear Titanium(IV)-oxo-iminodiacetate Cluster with Ti_6O_9 Core: Single-Crystal Structure and Photocatalytic Activities.

Lubin Ni^a, Dashuai Liang^a, Yin Cai^a, Guowang Diao^{*a}, Zhaohui Zhou^{*b}

Contents

Table S1 Crystallographic data and structural refinements for $\{\text{Ti}_6\text{O}_9\}$ cluster	S2
Table S2. Selected bond distances for $\{\text{Ti}_6\text{O}_9\}$ cluster.	S3
Table S3. Comparisons of Ti—O and Ti—Ti bond distances in Å in the purely titanium(IV) -oxo-carboxylate complexes	S3
Table S4. Bond valence sums (BVS) for $\{\text{Ti}_6\text{O}_9\}$ cluster	S3
Figure S1. ORETP plot of $[\text{Ti}_6\text{O}_9(\text{idc})_6]^{6-}$ polyanion with 30% thermal ellipsoids probability.	S4
Figure S2. X-ray powder patterns of $\{\text{Ti}_6\text{O}_9\}$ cluster vs. calculated pattern.	S4
Figure S3. Thermogravimetric curves of $\{\text{Ti}_6\text{O}_9\}$ cluster.	S5
Figure S4. FT-IR spectra of $\{\text{Ti}_6\text{O}_9\}$ cluster in solid stat	S5
Figure S5. Solid state UV/vis spectra of $\{\text{Ti}_6\text{O}_9\}$ cluster.	S6
Figure S6. Cyclic voltammograms of 0.1 mM $\{\text{Ti}_6\text{O}_9\}$ cluster.	S6
Figure S7. ^{13}C NMR spectra of the solutions of $\text{K}_2(\text{idc})$ at various pH values.	S7
Figure S8. Negative ion electrospray ionization mass spectra (ESI-MS) of $\{\text{Ti}_6\text{O}_9\}$ cluster in $\text{H}_2\text{O}/\text{MeCN}$ (80:20) solution	S7
Figure S9. UV-Vis time dependent absorption spectrum during photocatalytic reaction of RhB in the presence and absence of $\{\text{Ti}_6\text{O}_9\}$ cluster	S8

Table S1. Crystallographic data and structural refinements for $\{\text{Ti}_6\text{O}_9\}$ cluster.

$\{\text{Ti}_6\text{O}_9\}$	
Empirical formula	$\text{C}_{24}\text{H}_{56}\text{Cl}_2\text{K}_7\text{N}_6\text{O}_{46}\text{Ti}_6$
Formula weight (g·mol ⁻¹)	1796.75
Temperature (K)	293(2)
Wavelength (Å)	0.71069
crystal system, S. G.	Hexagonal, <i>P63/mcm</i>
a (Å)	13.067(5)
b (Å)	13.067(5)
c (Å)	24.283(5)
α (deg)	90
β (deg)	90
γ (deg)	120
volume (Å ³)	3591(2)
Completeness	97.8 % % (to $\theta = 26.37^\circ$)
Z	2
Abs coefficient (mm ⁻¹)	1.217
d _(calcd.) (Mg·m ⁻³)	1.662
F(000)	1818
Crystal size (mm ³)	0.20×0.18×0.10
GOF on F ²	1.087
Reflections collected / unique	16061 / 1338 [$R_{(int)} = 0.0270$]
Final $R_I[I > 2\sigma(I)]$ ^[a]	0.0521
wR ₂ indices [$I > 2\sigma(I)$] ^[b]	0.1579

[a] $R_I = \sum(\text{Fo} - \text{Fc})/\sum\text{Fo}$; [b] $wR_2 = \{\sum w(\text{Fo}^2 - \text{Fc}^2)^2/\sum w(\text{Fo}^2)^2\}^{1/2}$

Table S2. Selected bond lengths (\AA) and angles ($^\circ$) for $\{\text{Ti}_6\text{O}_9\}$ cluster.

Ti(1)-O(4)	1.8127(8)	Ti(1)-O(3a)	1.8293(15)	Ti(1)-O(3)	1.8295(13)
Ti(1)-O(1b)	2.096(3)	Ti(1)-O(1)	2.096(3)	Ti(1)-N(1)	2.252(3)
Ti(1)-Ti(1a)	3.3709(18)	Ti(1)-Ti(1c)	3.3709(18)		
O(4)-Ti(1)-O(3a)	103.31(15)	O(4)-Ti(1)-O(3)	103.31(15)	O(3a)-Ti(1)-O(3)	97.2(2)
O(4)-Ti(1)-O(1b)	89.00(14)	O(3a)-Ti(1)-O(1b)	88.19(13)	O(3)-Ti(1)-O(1b)	164.93(12)
O(4)-Ti(1)-O(1)	89.00(14)	O(3a)-Ti(1)-O(1)	164.93(12)	O(3)-Ti(1)-O(1)	88.19(13)
O(1b)-Ti(1)-O(1)	83.32(16)	O(4)-Ti(1)-N(1)	159.2(2)	O(3a)-Ti(1)-N(1)	90.29(13)
O(3)-Ti(1)-N(1)	90.29(13)	O(1b)-Ti(1)-N(1)	75.57(11)	O(1)-Ti(1)-N(1)	75.57(11)
O(4)-Ti(1)-Ti(1c)	92.53(15)	O(3a)-Ti(1)-Ti(1)	80.14(10)	O(3)-Ti(1)-Ti(1)	22.87(10)
O(1b)-Ti(1)-Ti(1c)	168.27(8)	O(1)-Ti(1)-Ti(1c)	108.33(8)	N(1)-Ti(1)-Ti(1c)	105.44(10)
O(4)-Ti(1)-Ti(1a)	92.53(15)	O(3a)-Ti(1)-Ti(1)	22.87(10)	O(3)-Ti(1)-Ti(1a)	80.14(10)
O(1b)-Ti(1)-Ti(1a)	108.33(8)	O(1)-Ti(1)-Ti(1a)	168.27(8)	N(1)-Ti(1)-Ti(1a)	105.44(10)
Ti(1c)-Ti(1)-Ti(1a)	60.0				

Symmetry transformation for $\{\text{Ti}_6\text{O}_9\}$ cluster: *a*, -*y,x-y,z*; *b*, *x-y,-y,z*; *c*, -*x+y,-x,z***Table S3.** Comparisons of the average Ti–O and Ti–Ti bond distances (\AA) in the purely titanium(IV)-oxo-carboxylate complexes.

	${}^{\text{av}}\text{Ti}-\text{O}_{\text{bridg}}$	${}^{\text{av}}\text{Ti}-\text{O}_{\text{carboxy}}$	${}^{\text{av}}\text{Ti}-\text{N}$	${}^{\text{av}}\text{Ti}-\text{Ti}$
$(\text{NH}_4)_4[\text{Ti}_2(\text{O}_2)_2(\text{C}_6\text{H}_4\text{O}_7)_2]\cdot 2\text{H}_2\text{O}$ [11a]	1.871(2)	2.038(2)	/	3.336(1)
$[\text{Ti}_4\text{O}_4(\text{C}_2\text{O}_4)_8]\cdot 4\text{C}_2\text{N}_2\text{H}_{10}\cdot 4\text{H}_2\text{O}$ [11d]	1.812(2)	2.071(2)	/	
$\text{Cs}_4[\text{Ti}_4\text{O}_4(\text{nta})_4]\cdot 6\text{H}_2\text{O}$ [11b]	1.831(2)	1.981(2)	2.292(2)	
$\text{Cs}_2\text{H}_2[(\text{Ti}_8\text{O}_8)(\mu-\text{dptaO})_4]\cdot 12\text{H}_2\text{O}$ [11c]	1.817(8)	2.029(9)	2.28(1)	/
$[\text{Ti}_8\text{O}_{10}(\text{OOCR})_{12}]$ [R = $\text{CH}(\text{CH}_3)_2$, CCl_3] [11f]	1.83	2.06	/	/
$[\text{Ti}_8\text{O}_8(\text{OOCR})_{16}]$ [R= C_6H_5 , $\text{C}(\text{CH}_3)_3$, CH_3] [11e]	1.8264(2)	2.0539(3)	/	/
$[\text{Ti}_8\text{O}_{10}(\text{citrate})_4(\text{H}_2\text{O})_{12}] \cdot 14\text{H}_2\text{O} \cdot 3(\text{HoPr})$ [11g]	1.894(3)	2.055(3)	/	3.63
$[\text{Ti}_8\text{O}_8(\text{OH})_4(\text{O}_2\text{CC}_6\text{H}_4\text{CO}_2)_6]$	1.915(5)	1.98(1)	/	
$\text{K}_7\text{H}[\text{Ti}_6\text{O}_9(\text{ida})_6]\text{Cl}_2 \cdot 20\text{H}_2\text{O}$ $\{\text{Ti}_6\text{O}_9\}$ (This work)	1.8208(10)	2.096(2)	2.252(3))	3.3703(17)

Table S4. Bond valence sums (BVS) for $\{\text{Ti}_6\text{O}_9\}$ cluster.

$\{\text{Ti}_6\text{O}_9\}$ cluster						
Ti1	4.0163	O1	2.2178	O2	1.7376	O3
O4	1.8997					1.9131

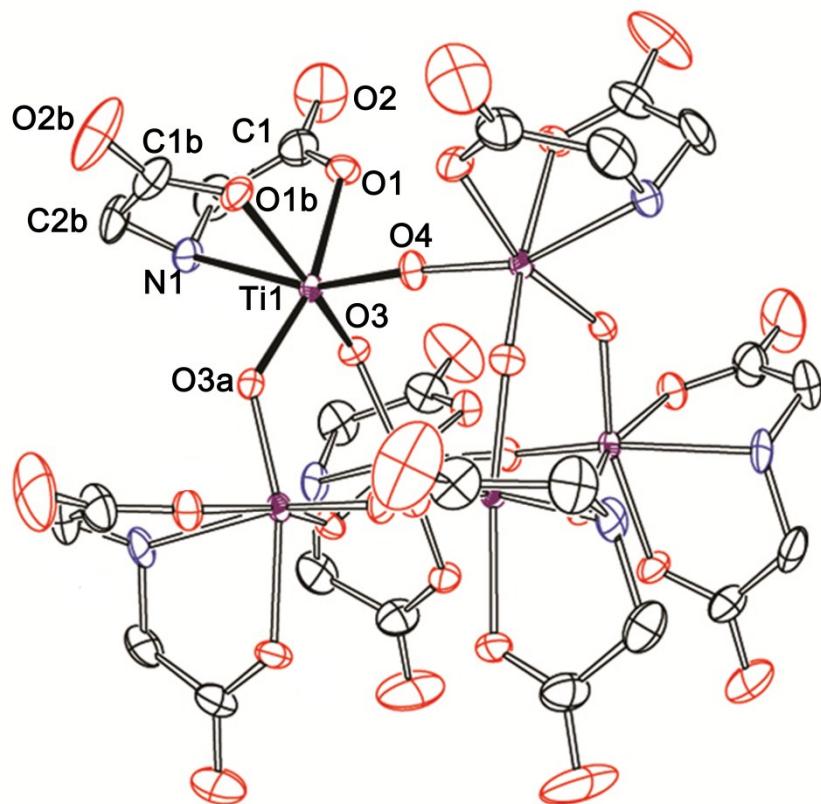


Figure S1. ORETP plot of $[\text{Ti}_6\text{O}_9(\text{ida})_6]^{6-}$ polyanion with 30% thermal ellipsoids probability. hydrogen atoms have been omitted for clarity. (color code: Ti: pink; O: red; N: blue; C: black; symmetry codes: a , $-y$, $x-y$, z ; b , $x-y$, $-y$, z ; c , $-x+y$, $-x$, z).

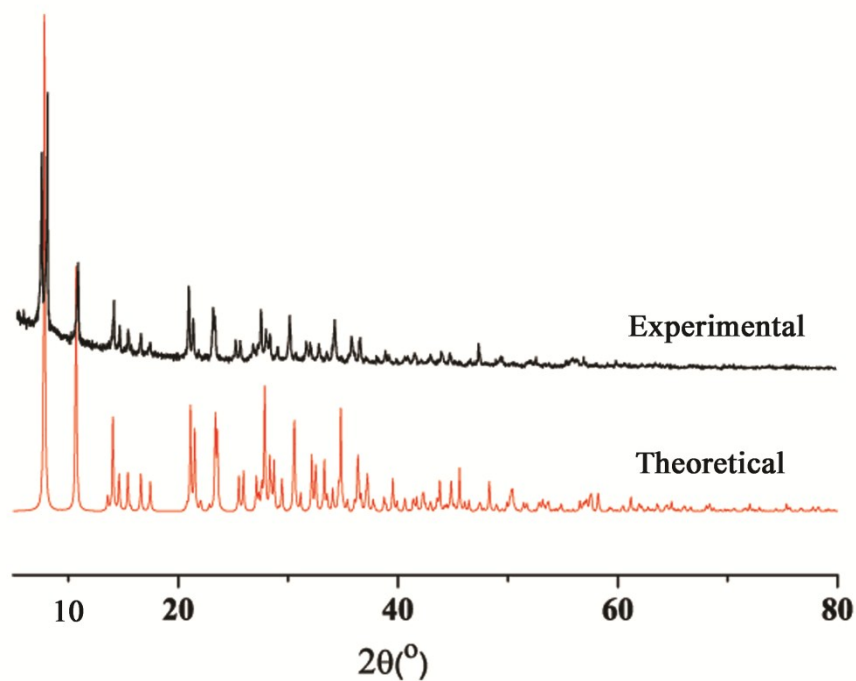


Figure S2. X-ray powder diffraction pattern of bulk $\{\text{Ti}_6\text{O}_9\}$ cluster vs. the calculated pattern. Peak positions are in good agreement, indicating the phase purity of the compound. Differences in intensity are due to preferred orientation of the powder sample.

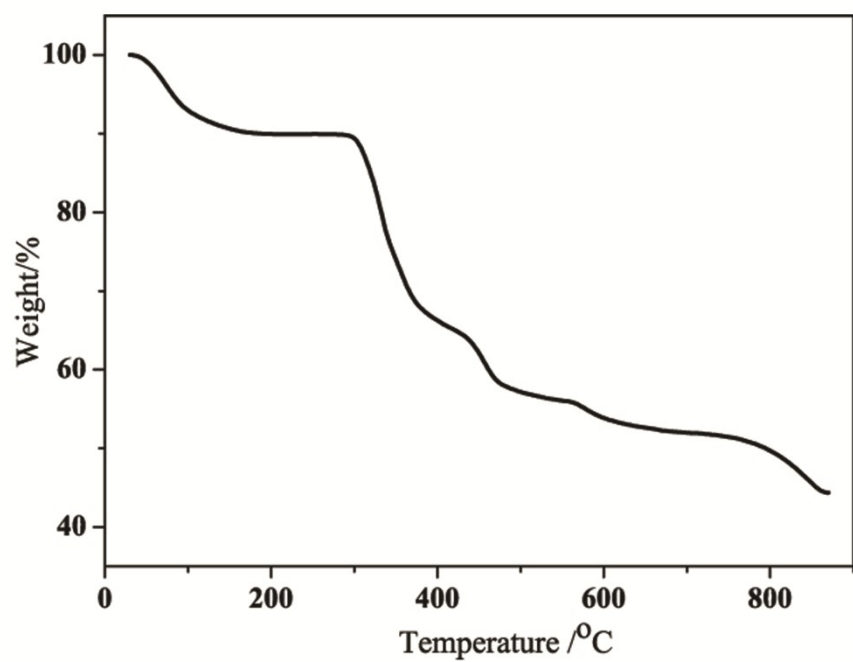


Figure S3. Thermogravimetric curves of $\{\text{Ti}_6\text{O}_9\}$ compound.

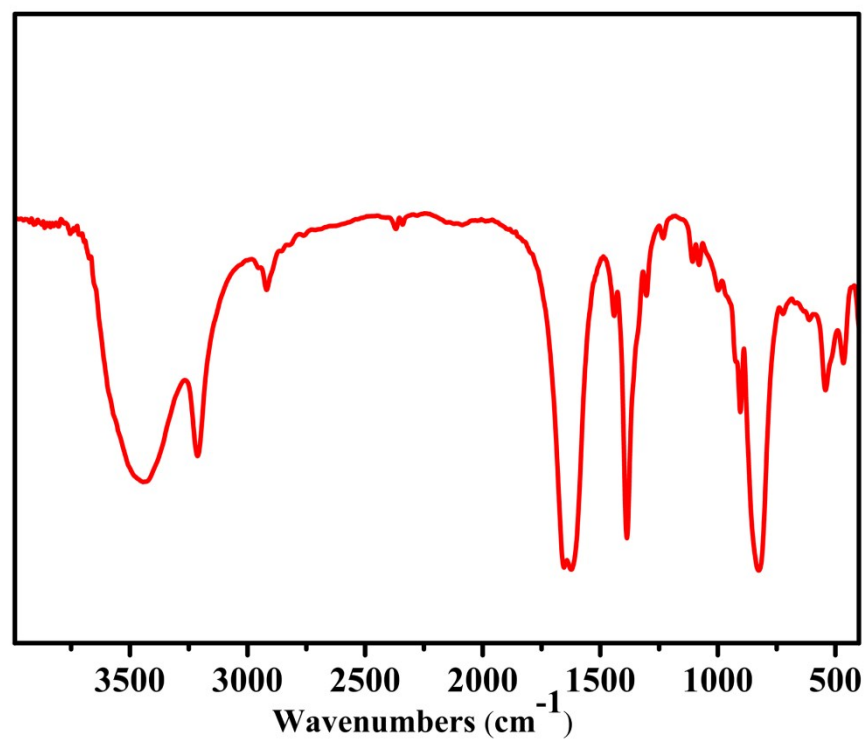


Figure S4. FT-IR spectra of $\{\text{Ti}_6\text{O}_9\}$ cluster in solid state.

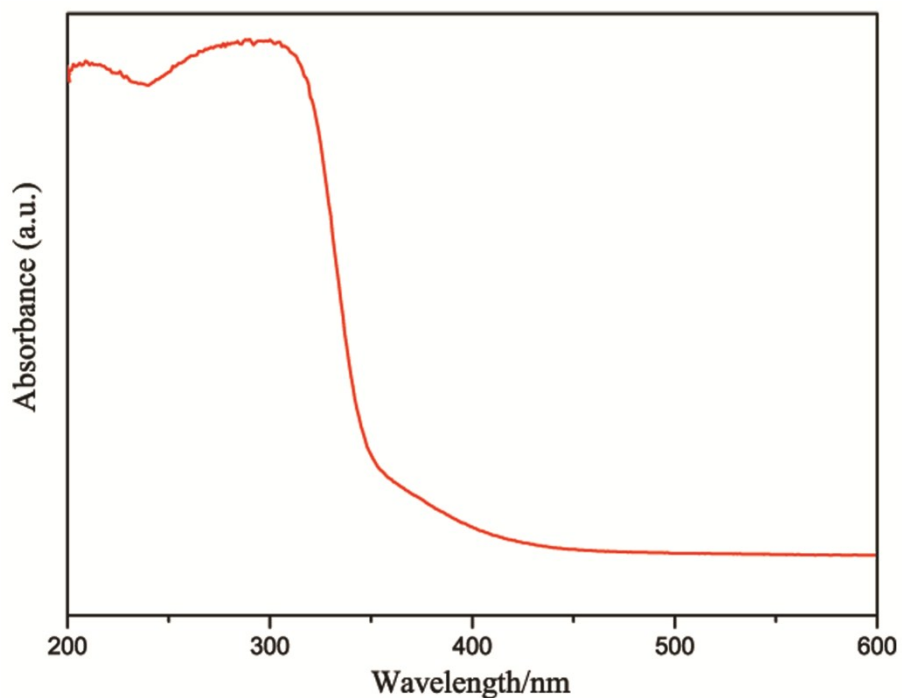


Figure S5. Solid state UV/vis spectra of $\{Ti_6O_9\}$ cluster. (Band gap: E_g (eV) = $hc / \lambda \approx 1240 / \lambda_{onset}$, h Planck's constant; c the speed of light in vacuum.

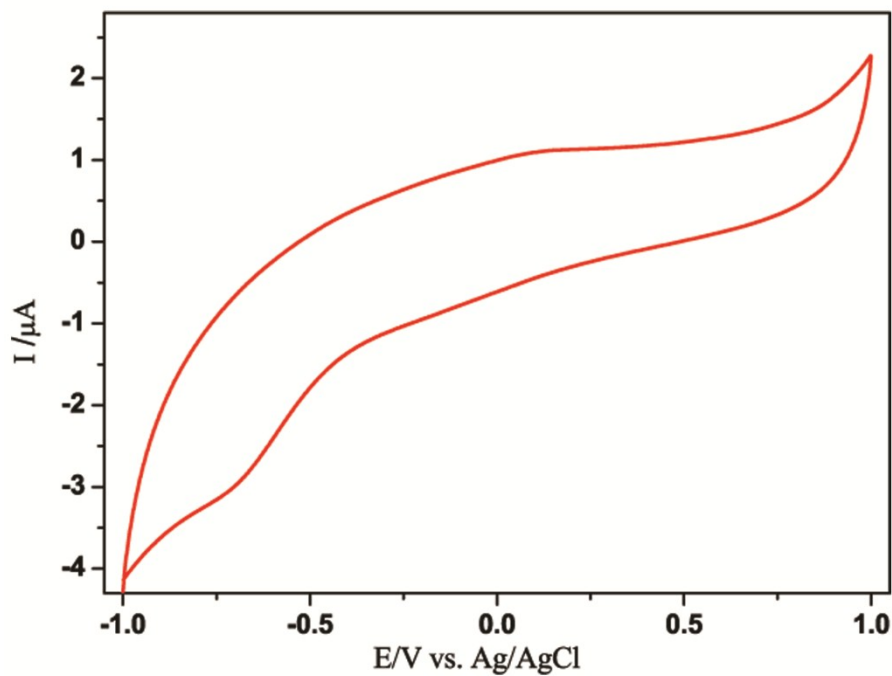


Figure S6. Cyclic voltammograms of 2 mM $\{Ti_6O_9\}$ compound in aqueous solution (scan rate 25 mV/s, GCE working electrode, Ag/AgCl reference electrode).

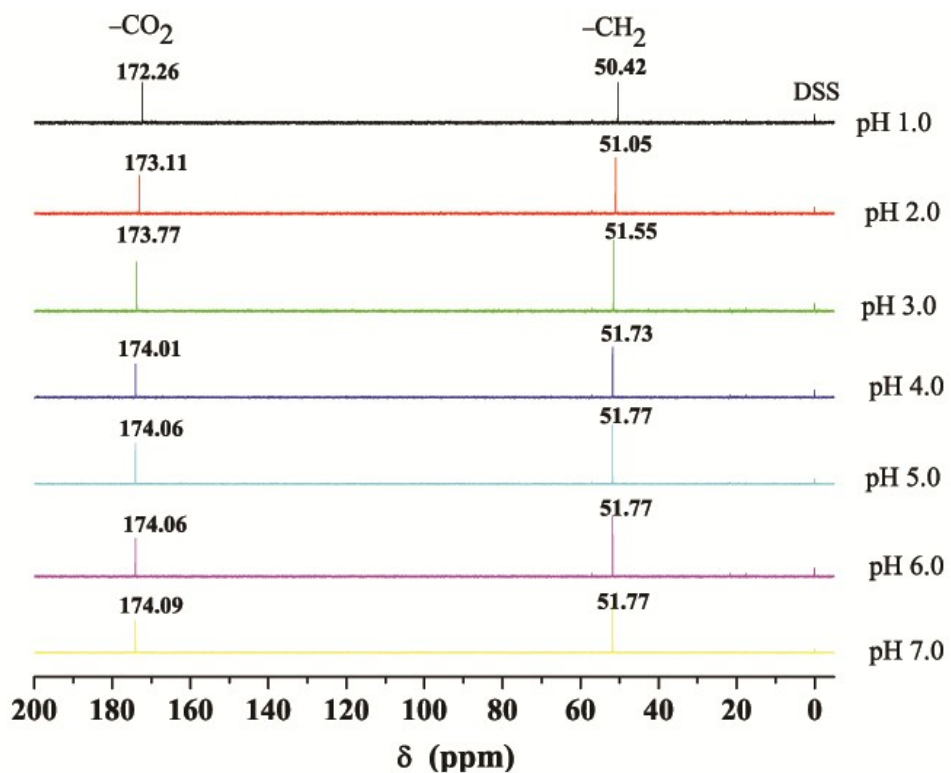


Figure S7. ^{13}C NMR spectra of the solutions of $\text{K}_2(\text{ida})$ at various pH values.

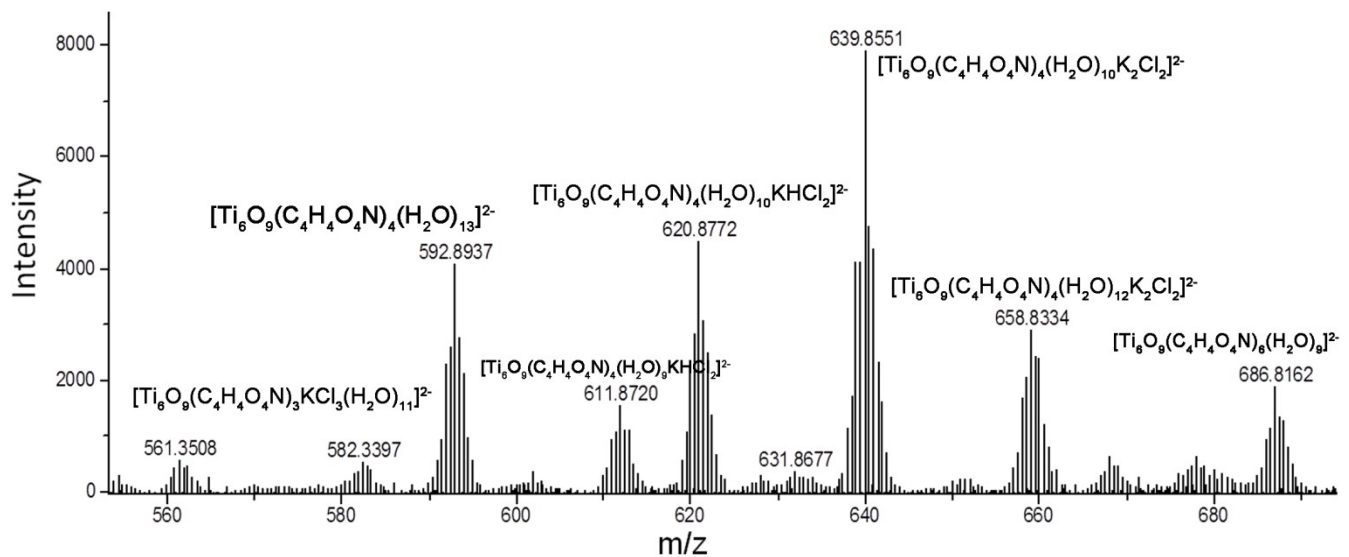


Figure S8. Negative ion electrospray ionization mass spectra (ESI-MS) of $\{\text{Ti}_6\text{O}_9\}$ cluster in $\text{H}_2\text{O}/\text{MeCN}$ (80:20) solution.

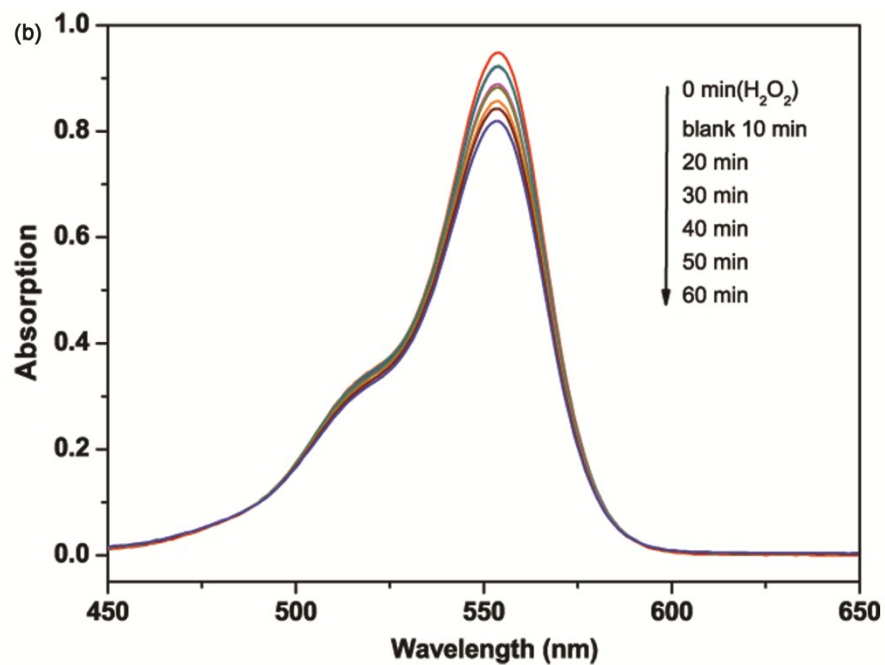


Figure S9. Absorption spectra of RhB during the degradation under visible light only with H_2O_2 (2mL, 20mmol).